

# Hadronic Final States and QCD: Summary

Thomas Gehrmann<sup>1</sup>, Günter Grindhammer<sup>2</sup>, Vivian O'Dell<sup>3</sup> and Roman Walczak<sup>4</sup>

1- Institut für Theoretische Physik, Universität Zürich, CH-8057 Zürich, Switzerland

2- Max-Planck-Institut für Physik, Föhringer Ring 6, D-80805 München, Germany

3- Fermilab, Batavia, IL 60510-0500, USA

4- Oxford University, Keble Road, Oxford OX1 3RH, UK

A summary of new experimental results and recent theoretical developments discussed in the “Hadronic Final States and QCD” working group is presented.

## 1 Introduction

The study of hadronic final states at colliders provides a broad spectrum of insights on hadronic structure and spectroscopy and on the physics of quantum chromodynamics (QCD). Especially for lepton-hadron and hadron-hadron colliders, these results are crucial for the successful interpretation of any kind of measurement, since QCD effects are omnipresent due to the hadronic initial state. In this working group, a variety of new results on many different aspects of hadronic final states were presented. These are summarised in this talk.

## 2 Vector Boson Production

The measurement and modelling of inclusive single vector boson + jets production is both a test of perturbative QCD and is an important background measurement for new physics. Tevatron measurements of  $Z/\gamma^* + \text{jets}$  and  $W + \text{jets}$  were presented [1]. Figure 1 compares the measured inclusive jet cross section from events with a  $Z/\gamma^* \rightarrow e^+e^-$  to the next-to-leading order (NLO) QCD prediction (open circles). The measurement for  $N_{jet} \geq 1$  is scaled up (factor 20) for clarity. The shaded bands show the total systematic uncertainty except for the 5.8% luminosity uncertainty. The dashed and dotted lines indicate the uncertainty due to parton distribution functions (PDFs) and the scale variations of the NLO QCD predictions respectively.

The LHC will be a  $W/Z$  factory, producing roughly 20 million  $W$ 's and 2 million  $Z$ 's visible by the general purpose detectors in each  $\text{fb}^{-1}$  of data. The ATLAS experiment at the LHC has done detailed studies [2] using both PYTHIA and ALPGEN

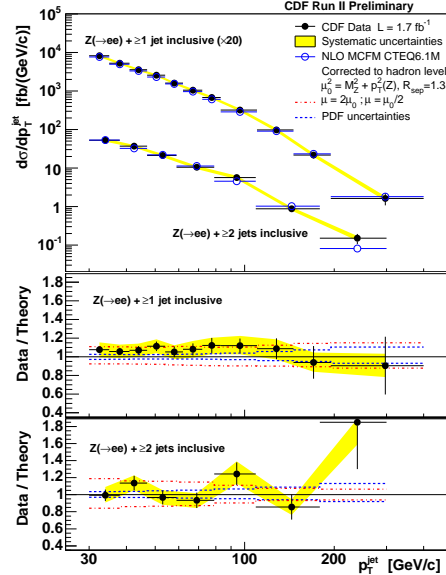


Figure 1: (a) Measured inclusive jet cross section as a function of  $p_T$  in  $Z/\gamma^* \rightarrow e^+e^- + \text{jets}$  events. Plots (b) and (c) show the data/theory ratio. Figure taken from [1].

Monte Carlo programs to extract predictions on reconstruction and trigger efficiency, background contributions and systematic uncertainties for  $W/Z + \text{jets}$  events. The dominant experimental uncertainty comes from the jet energy scale, and the ultimate ATLAS goal of 1% jet energy uncertainty would yield a systematic error of about 0.5% on the vector boson + jets cross sections.

For a Higgs boson mass  $M_H \gtrsim 2M_W$ , the most promising Higgs discovery channel at the Tevatron and the LHC is its decay into vector boson pairs. In the decay into  $W$ -bosons, no clear mass peak is observable, since the neutrino from the  $W$ -decay leaves the detector unobserved. To establish a Higgs boson discovery in this channel, a precise understanding of the Standard Model background processes yielding vector boson pairs is mandatory. At present, vector boson pair production is described theoretically at NLO. At this order, vector boson pairs are produced from quark-antiquark annihilation and quark-gluon scattering. Gluon-gluon fusion into vector boson pairs contributes only at next-to-next-to-leading order (NNLO), but could yield a potentially large contribution at the LHC because of the large gluon luminosity.

The NNLO gluon-gluon fusion contribution to vector boson pairs production was recently computed in [3], including all vector boson decay information. Although gluon-gluon fusion contributes only four per cent to the total vector boson pair production cross section, its importance is substantially enhanced to above ten per cent by particle reconstruction cuts, and further to thirty per cent by Higgs boson search cuts. This observation clearly highlights the need for a full NNLO calculation of vector boson pair production. First steps in this direction have recently been completed with the calculation of the two-loop and one-loop squared corrections [4] to the quark-antiquark annihilation matrix elements in the high energy limit.

### 3 Underlying Event

The term “underlying event” summarises all event activity which is observed besides the hard interaction, for example: multiple interactions, event pile-up and remnant interactions. Since this underlying activity results typically only in low-momentum particles, it is not accessible to a fully perturbative description (although at least multiple interactions may be calculable in the high energy limit [5]). At present, the description of the underlying event in Monte Carlo generator programs is based on models, such as the eikonal model of multiple scattering [6] which is used in HERWIG++ [7]. These models require tuning to experimental data, and their extrapolation from Tevatron to LHC energies is highly uncertain.

In order to study and fit the underlying event in data, regions can be defined where the underlying event contribution is enhanced. Figure 2 shows an example of dividing Tevatron Drell-Yan events into three regions with respect to the  $\phi$  direction of the lepton pair [8]: the “toward” direction is defined as a cone within  $\Delta\phi < 60^\circ$  to the  $Z$  boson, the “away” direction is defined as a cone within  $\Delta\phi < 60^\circ$  in the opposite direction, and the “transverse”

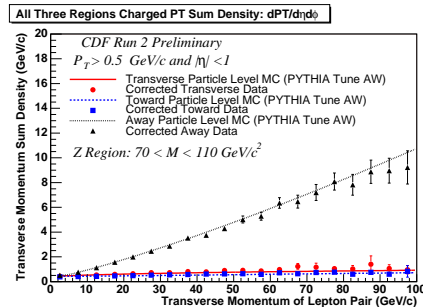


Figure 2: Underlying event study in vector boson production at CDF. Figure taken from [8].

direction, which is very sensitive to the underlying event, is defined as the remaining area. The three regions are compared to PYTHIA, tuned to a similar analysis using high  $p_T$  jet events (PYTHIA tune AW), and show good agreement.

The impact of the underlying event will be much larger at the LHC, where one expects roughly 35 minimum bias events per bunch crossing at the design luminosity of  $10^{34} \text{ cm}^{-2}\text{s}^{-1}$ . The CMS experiment presented plans [9] for measuring the minimum-bias contribution using a dedicated forward hadronic trigger and also presented studies of the remnant interactions besides the hard scattering, using the same analysis strategy as at the Tevatron. These studies are part of an overall strategy to quickly tune and understand QCD reactions at the new energy frontier.

## 4 Monte Carlo Tools

Event generator programs are based on leading order matrix elements, describing a primary (low multiplicity) hard scattering process, which is then used as input to a parton-shower to generate higher multiplicities. The resulting multi-parton final state is then transformed into a multi-hadron final state using a hadronisation model. Based on Monte Carlo algorithms, these programs provide samples of unweighted events, which can then be further processed using detector simulation and event reconstruction software. They are employed very widely in all aspects of experimental studies at particle colliders. The programs which are currently used most extensively were initially developed about twenty years ago and have undergone continuous upgrades. Nevertheless, these programs now start to display serious shortcomings, since a variety of new theoretical developments (for example, the matching of leading order multi-particle matrix elements onto the parton shower, or higher order corrections or improved shower prescriptions) cannot be incorporated into them. To overcome these limitations, several completely new Monte Carlo codes are currently being developed.

The HERWIG++ project [10] is a new Monte Carlo generator program, aiming to incorporate the ideas of the well-established HERWIG generator, which was most widely used in the previous generation of collider experiments. Its new fully functional release became available recently, and it includes, among other improvements, standard interfaces to specialised matrix element generators, simulation of a variety of beyond-Standard-Model reactions, a consistent treatment of radiation off heavy particles, and the simulation of underlying event dynamics [11] using an eikonal model [6].

The SHERPA project [12] is a newly developed Monte Carlo generator program, aiming to incorporate many of the recent new theoretical developments: recent additions in this project include the merging of multi-parton matrix elements with parton showers [13], a new shower model based on the dipole formalism [14], preparations for automated NLO calculations [15], and a new matrix-element generator based on improved Berends-Giele recursion relations [16].

All generic multi-purpose Monte Carlo programs are at present restricted to leading order in perturbative QCD. The extension of Monte Carlo programs to include NLO corrections is a currently ongoing activity, and has been accomplished for a variety of specific processes already [17]. For internal consistency, leading order Monte Carlo programs should use parton distribution functions at leading order. In fitting LO parton distributions to deep inelastic scattering and hadron collider data, one observes a poor fit quality, largely due to the high precision of the experimental data, which are sensitive to higher order QCD effects in the different observables. To improve the quality of the LO description of data on the proton

structure, various modifications were suggested [18]: by easing the momentum sum rule and modifying the scale in the QCD evolution, it is possible to mimic some of the numerically dominant higher order effects. An alternative approach emerging from discussions in the working group would be to consider the parton distribution functions to be an integral part of each Monte Carlo event generator, and to include them as parameters to be tuned.

## 5 QCD in the High Energy Limit

In the conventional fixed-order approach to perturbative QCD, scattering cross sections are computed as expansion in the strong coupling constant, and the structure of incoming hadrons is described by parton distributions obtained within collinear factorisation, evolving according to the DGLAP evolution equations. This fixed-order approach provides a very successful description of a broad range of observables, it becomes however inappropriate if higher-order terms in the coupling constant expansion are enhanced by large logarithmic corrections, which can spoil the convergence of the perturbative series. In these cases, an all-order resummation of the large logarithmic corrections is required to obtain reliable predictions. In the high energy limit of QCD scattering processes, which corresponds to low  $x$  in deep inelastic scattering, terms of the form  $\alpha_s^n \ln^m x$  can become potentially large at all orders, thereby invalidating the fixed-order expansion. In this limit, collinear factorisation, which assumes transverse-momentum ordering of initial state radiation, becomes equally inappropriate and should be replaced by transverse-momentum ( $k_T$ ) factorisation, yielding unintegrated parton distributions. The resummation of large logarithms in the high energy limit is accomplished by the BFKL evolution equation.

Since the inclusive proton structure function at HERA energies is not sufficiently sensitive to differences between the DGLAP and BFKL approaches, experimental studies of BFKL resummation effects focus largely on specific hadronic final states at small  $x$ . Especially the forward jet cross section has turned out to be very discriminative between different approaches.

Data on this observable, single, double and triple differential cross sections are in general only poorly described by NLO QCD. Among standard parton shower event generator programs, only ARIADNE agrees with observations [19, 20], after having been tuned to other HERA data. ARIADNE is based on the colour dipole model and exhibits BFKL-like parton showers unordered in  $k_T$ . Differential information may also be gained from azimuthal correlations of dijet production at low  $x$  [21], which is not fully described by NLO QCD as illustrated in Figure 3. This observable is potentially sensitive to the unintegrated gluon distribution [22], and may enter into a global determination of unintegrated parton distribution functions.

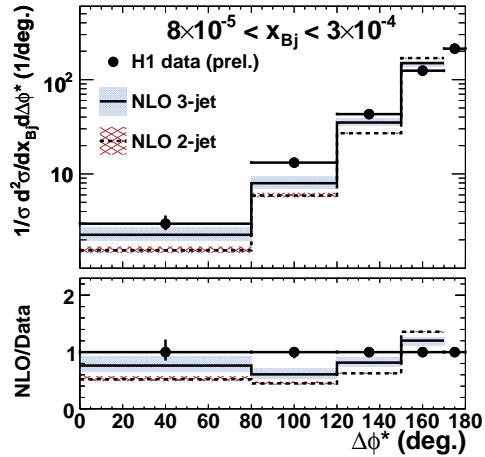


Figure 3: Dijet cross sections normalised to the visible cross section between  $0^\circ$  and  $170^\circ$  at HERA compared to NLO 3-jet and NLO 2-jet calculations. Figure taken from [21].

The BFKL equation at leading logarithmic (LL) approximation correctly describes the overall features of forward jet production. A fully reliable description can however only be attempted by including subleading logarithmic corrections (NLL), which are at present not yet fully available for jet production in deep inelastic scattering. An approximate NLL study [23] does show clear improvements upon BFKL at LL, such as a stabilisation of the scale and scheme dependence and agreement with experimental data from H1 over an extended kinematical range.

To compute cross sections within  $k_T$ -factorisation, one needs to derive scattering amplitudes with off-shell initial state partons. To obtain those in a gauge-invariant form, it is most convenient to couple the off-shell partons to an external current [24]. Recent calculations in this framework have focused in particular on final-state photon production [25, 26] in proton-proton and photon-proton collisions. Since these calculations do not provide the full final state information on all partons, issues like photon isolation and infrared cut-offs are still controversial.

The BFKL evolution equation at leading logarithmic accuracy can be reformulated as a parton shower by interpreting its evolution kernel as splitting probability [27]. In this formulation, constraints from energy-momentum conservation are implemented in a straightforward manner. The unintegrated parton distribution functions required as initial conditions are inferred from ordinary DGLAP parton distributions by undoing the last branching in the DGLAP evolution. With this parton shower formulation, leading logarithmic BFKL predictions can be made for a great variety of observables. For example, inclusive jet production at the Tevatron is correctly described over a wide kinematical range, Figure 4. It can be clearly seen that in certain kinematical regions different jet multiplicities can be of comparable numerical magnitude in the BFKL approach.

The BFKL formalism can also be applied directly to approximate the matrix elements for hard scattering needed for the prediction of multi-jet events. When supplemented by simple constraints on the analytic behaviour of the amplitudes [28], a good approximation of the corresponding full leading order matrix elements is achieved, while allowing for an all-order resummation of the hard perturbative corrections.

A complementary approach to the high-energy limit of QCD is the eikonal approximation, which allows to compute soft-gluon corrections to all orders in the coupling constant. This approximation is applied for example in pair production [29] of heavy quarks.

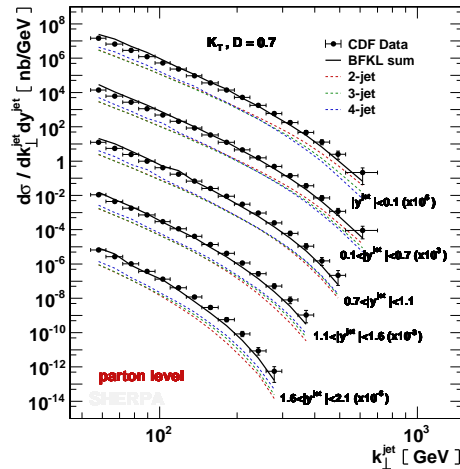


Figure 4: Inclusive jet cross sections at Tevatron compared to LL BFKL parton shower predictions. Figure taken from [27].

## 6 Hadron Spectroscopy

Hadron spectroscopy has been playing an important role in understanding strong interactions. Recently, ZEUS has studied  $K_S^0 K_S^0$  final states in  $ep$  collisions at HERA [30]. Three enhancements in invariant-mass distribution were observed, as shown in Figure 5. They correspond to  $f_2(1270)/a_2^0(1320)$ ,  $f_2'(1525)$  and  $f_0(1710)$  mesons. The interference pattern, predicted by SU(3) symmetry, was taken into account fitting the invariant-mass distribution. The  $f_0(1710)$  state, which has a mass consistent with a  $J^{PC} = 0^{++}$  glueball candidate, is observed with 5 standard-deviation statistical significance. However, if this state is the same as that seen in  $\gamma\gamma \rightarrow K_S^0 K_S^0$  [31] it is unlikely to be a pure glueball state.

A broad spectrum of results on hadronic interactions at low energies, including nuclear form factors and resonances [32] and colour transparency [33] is currently being obtained at TJNAF.

## 7 Heavy-Ion Collisions

At the Relativistic Heavy-Ion Collider, jets have been used to study the high energy density matter created in nuclear collisions. Defining regions in a similar way as in underlying event studies in  $p\bar{p}$  collisions, one can study the jet evolution in the quark matter. Figure [34] compares the jet evolution in  $pp$  and Au-Au collisions for increasing jet energy (here a jet is defined as a high energy hadron). In this figure, solid histograms (shaded bands) indicate elliptic flow model uncertainties. Arrows in (c) show the “head” region (HR) the “shoulder” region (SR) and the “near-side” region (NR). The  $pp$  data shows a typical two peak structure due to back to back dijets. The Au-Au spectra reveal jet quenching in the medium as the  $p_T$  increases, and in addition, they show a more complicated jet structure evolution with  $p_T$ , with prominent peaks in the “shoulder” regions at fixed positions – a feature expected from a medium-induced Mach shock.

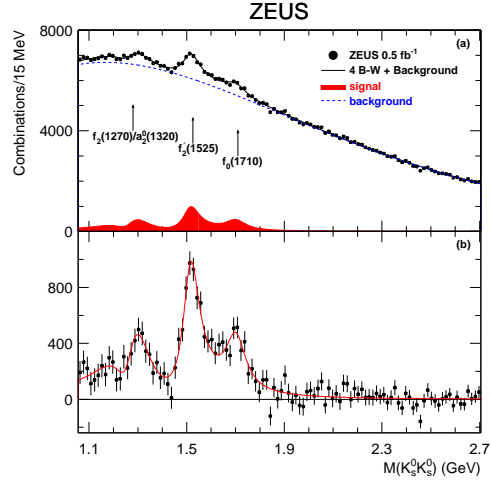


Figure 5: The measured  $K_S^0 K_S^0$  invariant-mass distribution. Figure taken from [30].

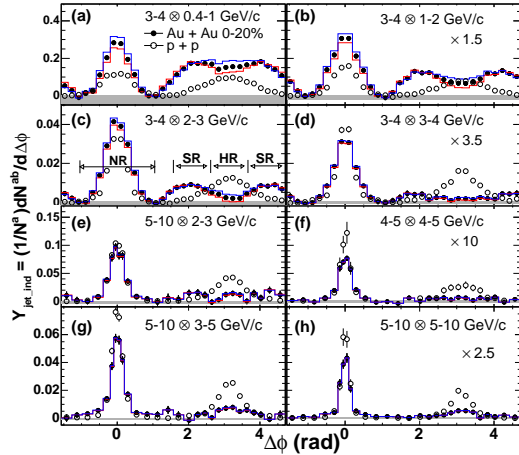


Figure 6: Per-trigger yield versus  $\Delta\phi$  for various trigger and partner  $p_T$  arranged by increasing pair proxy energy. Figure taken from [34].

## 8 Hadron Fragmentation

Charged particle production in DIS at HERA was studied in terms of multiplicity and scaled momentum distributions [35, 36]. When an appropriate energy scale is used,  $ep$  data can be consistently compared with data from  $e^+e^-$ ,  $\mu p$  and  $\nu p$  scattering over a wide energy range. In all cases, similar behaviour is observed, supporting quark fragmentation universality, see Figure 7.

Models, implemented in LO matrix element Monte Carlo programs, describe data reasonably well but NLO QCD calculations, using three different fragmentation functions, fail to describe the scaling violations seen in the data [36], see Figure 8.

The production of  $K_S^0$ ,  $\Lambda$  and  $\bar{\Lambda}$  in DIS at HERA has been investigated by H1 [37]. The model predictions, based on leading order Monte Carlo programs in general are able to describe the overall features of the measurements, however they fail in details, in particular in describing  $\Lambda$  and  $\bar{\Lambda}$  production in the current region of the Breit frame. It was also found that a constant strangeness fraction in hadron fragmentation fails to fit all the data.

Data from  $pp$ ,  $e^+e^-$  and heavy ion scattering has been used to test the limiting fragmentation hypothesis [38], and a prediction has been made for  $ep$  DIS [39].

Bose-Einstein correlations of hadron pairs at HERA have been studied by HERMES [40] for nuclear targets ranging from hydrogen to xenon. It was found that the parameters describing the correlations neither depend on the nuclear target nor on the hadronic invariant-mass.

Momentum distributions of identified hadrons can be used to extract hadron fragmentation functions, which describe the differential probabilities for specific parton-to-hadron transitions. These fragmentation functions obey DGLAP evolution equations with timelike splitting functions. At present, these timelike splitting functions are known to NLO, and calculations to NNLO are in progress [41]. Using extensive data sets taken in  $e^+e^-$ ,  $pp$  and  $p\bar{p}$  collisions, and including hadron mass corrections, a new global extraction of parton fragmentation functions to  $\pi^\pm$ ,  $K^\pm$ ,  $p/\bar{p}$ ,  $K_S^0$  and  $\Lambda/\bar{\Lambda}$  was performed recently [42]. Compared to earlier studies, especially the determination of non-singlet quark fragmentation functions is improved by charge asymmetry  $pp$  data from RHIC. Unfortunately, data on momentum distributions of identified light hadrons from HERA have up to now only

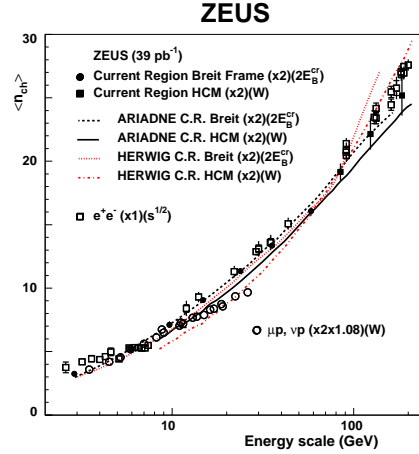


Figure 7: Mean charged multiplicity. Figure taken from [35].

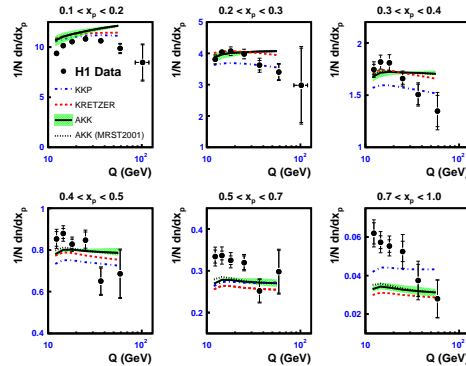


Figure 8: Normalised distributions of the scaled momentum. Figure taken from [36].

been released by the fixed-target HERMES experiment, while H1 and ZEUS measurements of charged and neutral light hadron production released up to now were not suitable for the extraction of fragmentation functions.

## 9 Isolated Photons

Direct photons coming from the partonic hard scattering are a powerful probe of the dynamics of hard QCD interactions. At Tevatron energies, the direct photon + jet cross section measurement is sensitive to the gluon density and thus can be used to complement the HERA data quark on the gluon at low  $x$  by constraining the gluon contribution at large  $x$ . In addition, photon final states are predicted in new physics models such as SUSY, Extra Dimensions, Technicolour, etc. The DZero experiment has measured [43] the isolated (hence enhanced direct)  $\gamma$  + jet inclusive cross section in four regions of jet and photon rapidity and compared them with theory using JETPHOX [44] and CTEQ6.5M PDFs as shown in Figure 9. The two dotted lines show the effect of theoretical scale variations by a factor of two; the shaded region indicates the CTEQ6.5M PDF uncertainty, and the dashed and dashed-dotted lines show ratios of the JETPHOX predictions with MRST 2004, Alekhin and ZEUS 2005 PDF sets to CTEQ6.5M. The systematic uncertainties have large bin-to-bin correlations in  $p_T^\gamma$ . An additional 7.8% normalisation uncertainty on the data points is not shown.

While there is overall agreement with the theoretical prediction, and the theory successfully models the  $p_T$  distributions for the isolated  $\gamma$ +jet measurements at HERA, the theory does not describe well the  $p_T^\gamma$  dependence of the cross sections as measured in  $p\bar{p}$  at the Tevatron. Neither reasonable variations in fragmentation functions nor contributions from threshold resummation are able to improve the data description from theory. Clearly this is an important measurement to be understood in preparation for data taking at LHC.

First results on prompt photons in photoproduction by the H1 collaboration making use of the full HERA-II statistics were presented [45]. They cover the phase space  $5 < E_T^\gamma < 15$  GeV and  $-1.0 < \eta^\gamma < 2.4$  in the laboratory frame. The isolation criterion for the prompt photon is defined by the require-

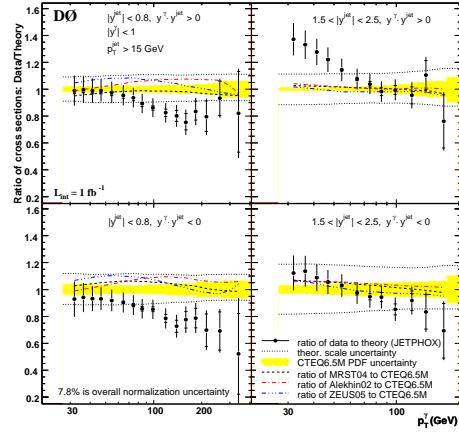


Figure 9: Ratio of measured and predicted cross section for  $p\bar{p} \rightarrow \gamma + jet + X$  as a function of  $p_T^\gamma$ . Figure taken from [43].

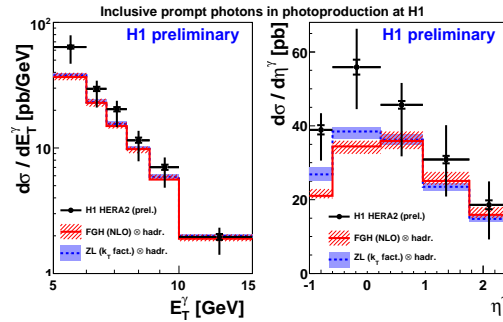


Figure 10: Inclusive prompt photons in photoproduction at HERA. Figure taken from [45].

ment that  $E_T^\gamma/E_T^{\gamma-jet} > 0.9$ . The data are above the two QCD predictions, particularly at low  $E_T^\gamma$  as can be seen in Figure 10. The FGH prediction [46] is based on collinear factorisation at NLO and the ZL prediction on a  $k_T$ -factorisation approach [47]. They equally investigated prompt photon plus jet data are found to be reasonably well described by both predictions, except at the highest  $x_\gamma^{obs}$ , where direct photoproduction is enhanced.

## 10 Precision Physics with Jets

Inclusive jet cross sections at  $p\bar{p}$  colliders are a sensitive probe of parton distribution functions and of new physics. The DZero experiment has made the most precise measurement of the inclusive jet cross section to date [48]. Figure 11 shows the ratio of the measured to predicted inclusive jet cross sections as a function of jet  $p_T$  in six rapidity bins. The theoretical prediction comes from a NLO QCD calculation using the CTEQ6.5 PDFs. The MRST2004 PDF predictions are also plotted. As is demonstrated in this figure, the experimental uncertainties are now smaller than the scale and PDF uncertainties. The dominant experimental uncertainty comes from the jet energy scale, and after seven years of work, the DZero collaboration has reduced this uncertainty to about 1.2% for high  $p_T$  central jets.

Studies are ongoing at the LHC in preparation for data taking in late 2008. New physics can be seen as one goes to higher  $p_T$  in the inclusive jet spectrum. The current limit on the contact interaction scale at the Tevatron is 2.7 TeV. The CMS experiment at the LHC will be able [49] to improve this limit within the first 10  $\text{pb}^{-1}$  of collected data. Assuming a jet energy scale uncertainty of 10% the predicted sensitivity to interaction scale is  $\Lambda \approx 3$  TeV, 7 TeV and 10 TeV for 10  $\text{pb}^{-1}$ , 100  $\text{pb}^{-1}$  and 1  $\text{fb}^{-1}$  respectively.

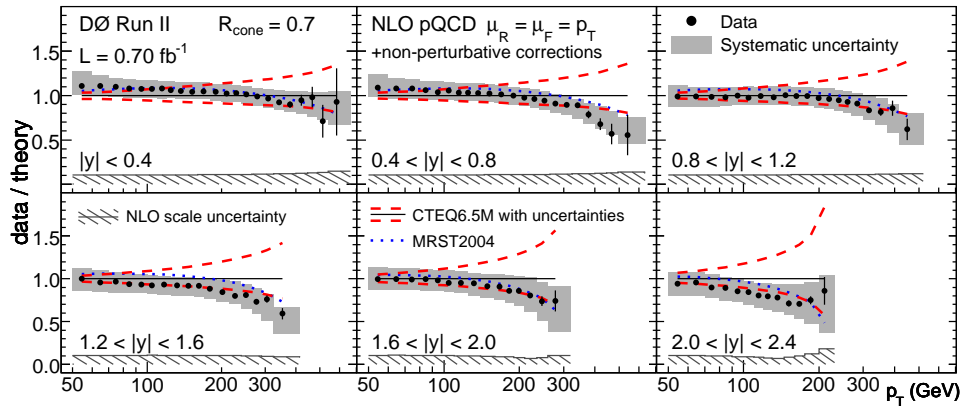


Figure 11: Inclusive jet cross section as measured by DZero divided by theory as a function of  $p_T$  for 6  $|y|$  bins. Measurement uncertainties are shown by the shaded bands and PDF uncertainties by the dashed lines. The theoretical prediction using the MRST2004 PDFs is shown by the dotted line. The hashed area at the bottom of the plots shows the uncertainty when varying the renormalisation and factorisation scales between  $p_T/2$  and  $2p_T$ . Figure taken from [48].

Recent measurements by the ZEUS collaboration of 2,3 and 4 jets in photoproduction were presented [50]. Compared to earlier 2-jet results, the jet transverse energy requirements ( $E_T^{jet(2)} > 20$  (15) GeV), the range in pseudorapidity ( $-1 < \eta^{jet} < 3$ ) and the luminosity have been significantly increased in order to obtain a dataset suitable for testing and constraining both the photon and the proton PDFs. The sensitivity to different PDFs was shown by comparing the data to different available parametrisations. For the 3 and 4-jets analysis the selection of the jet phase space was different:  $E_T^{jet} > 6$  GeV and  $|\eta^{jet}| < 2.4$ . In addition, the data were divided into a low and high mass sample with  $25 < M_{nj} < 50$  GeV and  $M_{nj} > 50$  GeV in order to look for effects of multi-parton interactions or underlying events and to allow for tests of multi-jet description in event generators. In general both models HERWIG and PYTHIA largely underestimate the rate of multi-jet events. At high  $M_{nj}$  however, they provide a reasonable description of the shape of the data, while low  $M_{nj}$  and low  $x_\gamma^{obs}$  are only described once multi-parton interactions are introduced. A leading order QCD calculation for 3-jets, corrected for hadronisation effects and effects of multi-parton interactions, is compared to data in Figure 12, illustrating the need for a NLO calculation.

For jets with sufficiently high  $E_T^{jet}$  one may expect the contribution of fragmentation to the jet substructure to become small compared to the contribution from parton radiation. Preliminary measurements by the ZEUS collaboration [51] of the mean integrated jet shape  $\langle \Psi(r) \rangle$  for two types of jets with  $14 < E_T^{jet} < 17$  GeV are in good agreement with corresponding NLO calculations as illustrated in Figure 13. The data are also well reproduced by the colour dipole model as implemented in ARIADNE. The “one-jet” distribution is mainly due to quark-initiated jets, selected by demanding events with 1-jet only. The “two-jet” distribution is enriched with gluon-initiated jets by choosing the jet with the lowest  $E_T^{jet}$  in events which have only two jets, which are close

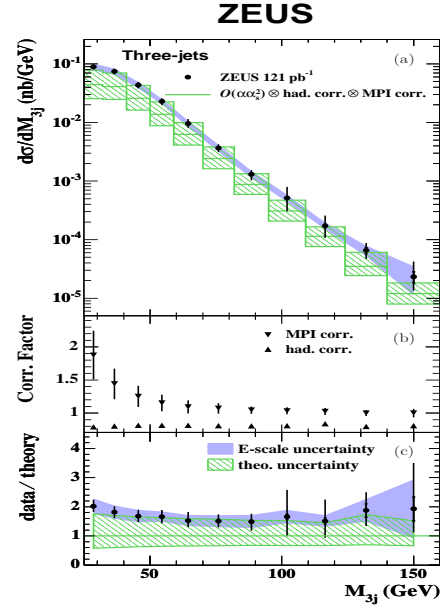


Figure 12: Photoproduction cross section of 3-jets as a function of the 3-jet invariant-mass at HERA. Figure taken from [50].

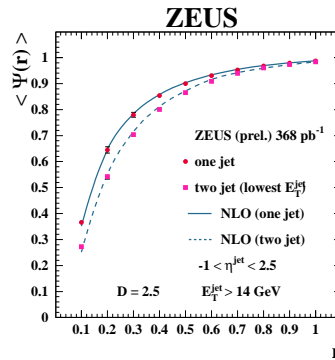


Figure 13: Integrated jet shapes for quark and gluon enriched jets in DIS at HERA. Figure taken from [51].

to each other in  $\eta - \phi$  space. One observes that the gluon enriched jets are broader as expected.

Recent polarised and unpolarised inclusive jet cross sections were measured by the ZEUS collaboration in charged current (CC)  $e^\pm p$  events using HERA-II data [52]. They are found to be in good agreement with Standard Model predictions. These jet cross sections and the fully inclusive CC cross sections can provide constraints on the  $u$  and  $d$ -PDFs at high  $x$ .

Preliminary results on normalised inclusive, 2-jet and 3-jet cross sections by the H1 collaboration were presented [53], using HERA-I and II data. In photon virtuality they cover the range  $5 < Q^2 < 15000 \text{ GeV}^2$  and in jet transverse energies  $7(5) < E_T^{jet} < 50(80) \text{ GeV}$ . The normalised inclusive jet cross section for the high  $Q^2$  data, i.e.  $Q^2 > 150 \text{ GeV}^2$ , is shown in Figure 14 together with published HERA-I data and NLO QCD calculations [54], illustrating good agreement and experimental errors, which are clearly smaller than the uncertainty of the NLO calculation. These high- $Q^2$  data have reached an experimental uncertainty of about 3 %, which is mainly due to the uncertainty of the jet energy scale of about 1.5 %.

The value of the strong coupling

$$\alpha_s(M_Z) = 0.1182 \pm 0.0008 \text{ (exp)}$$

$${}^{+0.0041}_{-0.0031} \text{ (theo)} \pm 0.0018 \text{ (PDF)}$$

was extracted from a fit of the NLO calculation to the normalised inclusive, 2 and 3-jet cross sections, resulting in an impressively small experimental error of 0.7 %. The total uncertainty is dominated by the uncertainty of the NLO theory, indicating the need for a NNLO calculation. The running of the strong coupling is verified over two orders of magnitude in  $Q$  as demonstrated in Figure 15.

Using the recently computed NNLO corrections to event shape variables [55], a new extraction of  $\alpha_s$  from data on the standard set of six event shape variables, measured [56] by the ALEPH collaboration at LEP1 and LEP2 was performed. One observes a clear improvement in the fit quality when going to NNLO accuracy [57]. Compared to NLO the value of  $\alpha_s$  is lowered by about 10%, but still higher than for NLO matched with the resummed next-to-leading logarithmic approximation (NLO+NLLA) [56]. As illustrated in Figure 16, the scatter among the  $\alpha_s$ -values extracted from different shape variables is lowered considerably, and the theoretical uncer-

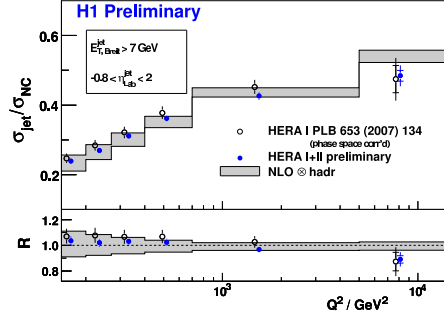


Figure 14: Normalised inclusive jet cross section and ratio of data over theory at HERA. Figure taken from [53].

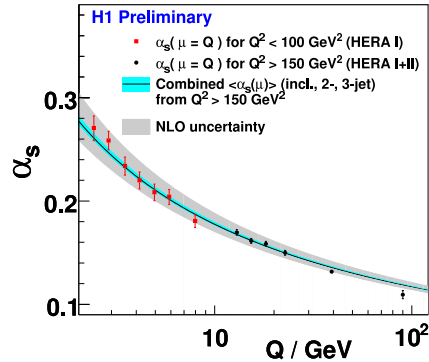


Figure 15: Running of  $\alpha_s$  from jet cross sections at HERA. Figure taken from [53].

tainty is decreased by a factor 2 (1.3) compared to NLO (NLO+NLLA). The combination of all shape variables at all energies yields

$$\alpha_s(M_Z) = 0.1240 \pm 0.0008(\text{stat}) \pm 0.0010(\text{exp}) \pm 0.0011(\text{had}) \pm 0.0029(\text{theo}).$$

The fixed-order QCD description of event shape distributions is reliable only if the event shape variable is sufficiently far away from its two-jet limit. In the approach to this limit, event shapes display large infrared logarithms at all orders in perturbation theory, such that the expansion in the strong coupling constant fails to converge. Resummation of these logarithms yields a description appropriate to the two-jet limit. To explain event shape distributions over their full kinematical range, both descriptions need to be matched onto each other. The matching of NLLA with NNLO was performed recently [58]. The most striking observation is that the difference between NLLA+NNLO and NNLO is largely restricted to the two-jet region, while NLLA+NLO differ in normalisation throughout the full kinematical range. This behaviour may serve as a first indication for the numerical smallness of corrections beyond NNLO in the three-jet region. Fits of  $\alpha_s$  based on NNLO+NLLA are currently in progress.

A summary of the most precise  $\alpha_s(M_Z)$  extractions from HERA data discussed at DIS 2008 is shown in Figure 17. It also includes the ‘‘HERA comb. 2007 incl. jets’’ result [59] of a first simultaneous fit to published HERA-I inclusive jet cross section data from H1 and ZEUS.

## 11 New Jet Algorithms

The reconstruction of hadronic jets at colliders proceeds through the application of a jet algorithm, which clusters the detector-level information on the hadrons (hadronic tracks or calorimeter energy deposits) into a limited number of composite objects: the jets. One distinguishes two types of jet algorithms: cone-based and cluster-based algorithms. The cone-based algorithms aim to maximise the hadronic energy inside a cone of fixed size, while the cluster-based algorithms perform a sequential recombination of parton pairs. For both classes of algorithms,

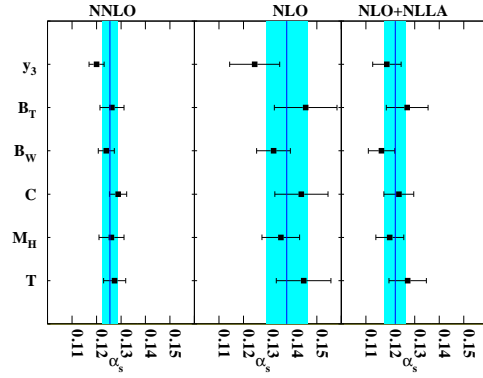


Figure 16: Strong coupling constant extracted from ALEPH data on event shapes. Figure taken from [57].

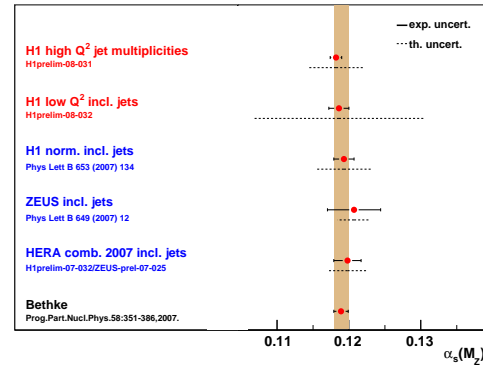


Figure 17: Summary of extractions of  $\alpha_s(M_Z)$  at DIS 2008.

many different realisations have been proposed in the past. Depending on the observable under consideration, one or the other type of algorithm may be more appropriate: while cone-type algorithms perform generally better in the reconstruction of resonances, i.e. in searches for massive particles decaying into jets, cluster-type algorithms are more appropriate for precision studies. To compare experimental jet measurements with perturbative QCD, any algorithm of either type must fulfil infrared safety criteria.

Unfortunately, most of the cone-based algorithms used up to now at the Tevatron did not fulfil those criteria and display infrared sensitivity above a certain final-state jet multiplicity. The principal cause of this infrared sensitivity is the use of cone seeds to speed up the jet reconstruction. The seedless infrared-safe cone algorithm (SISCone) [60] overcomes these problems and provides a cone-type algorithm for hadron collider physics.

The sequential recombination used in clustering-based algorithms is very time-consuming, since the distance measure for each pair of (pseudo-)particles has to be evaluated in each iteration. The practical applicability of these algorithms was therefore severely restricted, especially at hadron colliders, where typical events contain a very high multiplicity of hadronic objects. Using techniques from computational geometry, the clustering can be performed in a much more efficient way [61], such that cone-based and clustering algorithms display similar performance [62].

By generalising the  $k_T$ -clustering algorithm to allow arbitrary powers in the transverse momentum weight, one can define a one-parameter family of clustering algorithms. The weighting with the inverse power of the transverse momentum defines the anti- $k_T$  algorithm [63]. A new powerful tool to analyse the features of jets is their catchment area [64], which is obtained by including zero-energy ghost particles in the clustering. By inspecting the jet areas, one observes that the anti- $k_T$  algorithm yields perfect cones, which makes this algorithm an ideal replacement for iterative cone-type algorithms.

The jet area may be turned into a powerful tool to disentangle the hard scattering process from any underlying event activity. On an event-by-event basis, this underlying activity, which appears to be uniform in rapidity, could be measured in areas outside any jet, and then subtracted from the event prior to reconstruction. To illustrate the improvements which can be obtained using this procedure, Figure 18 displays the effect of event pileup on the reconstruction of the new heavy  $Z'$  gauge boson decaying into hadronic jets. While the mass peak is substantially shifted by the effect of pileup, it is observed at its true mass after jet area based subtraction.

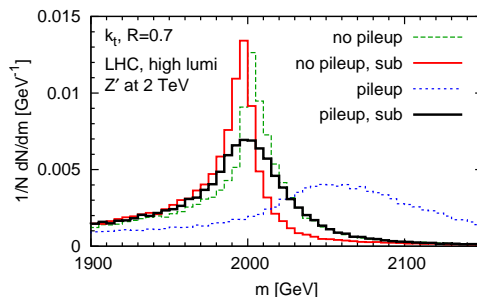


Figure 18: Effect of jet area based subtraction on reconstruction of heavy resonance at  $M = 2$  TeV decaying into jets. Figure taken from [64].

## 12 Conclusions

The broad spectrum of new results on “Hadronic final states and QCD” presented in the working group, as well as the very lively discussions, illustrate the importance of this subject area in the current transition period between HERA and the LHC. Many recent experimental

results are of direct relevance to preparations for LHC physics, and theoretical physics is responding to a number of challenges in complexity and precision posed by the physics programme of present and future colliders.

## Acknowledgment

TG would like to thank the Swiss National Science Foundation (SNF) for support under contract 200020-117602.

## References

- [1] T. Aaltonen *et al.*, [CDF collaboration], Phys. Rev. Lett. **100** (2008) 102001 and B. Cooper, these proceedings.
- [2] E. Dobson, these proceedings.
- [3] T. Binoth, M. Ciccolini, N. Kauer and M. Kramer, JHEP **0612** (2006) 046 [hep-ph/0611170]; T. Binoth, N. Kauer and P. Mertsch, these proceedings [arXiv:0807.0024].
- [4] G. Chachamis, M. Czakon and D. Eiras, arXiv:0802.4028; arXiv:0806.3043 and G. Chachamis, these proceedings.
- [5] J. Bartels, M. Salvadore and G.P. Vacca, JHEP **0806** (2008) 032 [arXiv:0802.2702].
- [6] I. Borozan and M.H. Seymour, JHEP **0209** (2002) 015 [hep-ph/0207283].
- [7] M. Bähr, J.M. Butterworth and M.H. Seymour, arXiv:0806.2949.
- [8] A. Metha, these proceedings.
- [9] F. Bechtel, these proceedings.
- [10] M. Bähr *et al.*, arXiv:0803.0883.
- [11] M. Bähr, S. Gieseke and M.H. Seymour, JHEP **0807** (2008) 076 [arXiv:0803.3633] and M. Bähr, these proceedings.
- [12] T. Gleisberg, S. Höche, F. Krauss, A. Schaliche, S. Schumann and J.C. Winter, JHEP **0402** (2004) 056 [hep-ph/0311263] and F. Krauss, these proceedings.
- [13] A. Schaliche and F. Krauss, JHEP **0507** (2005) 018 [hep-ph/0503281].
- [14] S. Schumann and F. Krauss, JHEP **0803** (2008) 038 [arXiv:0709.1027]; J.C. Winter and F. Krauss, JHEP **0807** (2008) 040 [arXiv:0712.3913].
- [15] T. Gleisberg and F. Krauss, Eur. Phys. J. C **53** (2008) 501 [arXiv:0709.2881].
- [16] C. Duhr, S. Höche and F. Maltoni, JHEP **0608** (2006) 062 [hep-ph/0607057] and S. Höche, these proceedings.
- [17] S. Frixione and B. R. Webber, JHEP **0206** (2002) 029 [hep-ph/0204244]; S. Frixione, P. Nason and C. Oleari, JHEP **0711** (2007) 070 [arXiv:0709.2092]; Z. Nagy and D. E. Soper, JHEP **0510** (2005) 024 [hep-ph/0503053].
- [18] A. Sherstnev and R.S. Thorne, Eur. Phys. J. C **55** (2008) 553 [arXiv:0711.2473] and A. Sherstnev, these proceedings.
- [19] S. Chekanov *et al.* [ZEUS Collaboration], Eur. Phys. J. C **52** (2007) 515 [arXiv:0707.3093] and L. Khein, these proceedings.
- [20] A. Aktas *et al.* [H1 Collaboration], Eur. Phys. J. C **46** (2006) 27 [hep-ex/0508055].
- [21] J. Turnau, these proceedings.
- [22] F. Hautmann, these proceedings.
- [23] O. Kepka, C. Royon, C. Marquet and R.B. Peschanski, Eur. Phys. J. C **55** (2008) 259 [hep-ph/0612261] and C. Royon, these proceedings.
- [24] K. Kutak, these proceedings.

- [25] S.P. Baranov, A.V. Lipatov and N.P. Zotov, Phys. Rev. D **77** (2008) 074024 [arXiv:0708.3560] and N.P. Zotov, these proceedings.
- [26] V.A. Saleev, these proceedings.
- [27] S. Höche, F. Krauss and T. Teubner, arXiv:0705.4577 and S. Höche, these proceedings.
- [28] J.R. Andersen and C.D. White, arXiv:0802.2858 and C.D. White, these proceedings.
- [29] N. Kidonakis, A. Sabio Vera and P. Stephens, arXiv:0802.4240 and N. Kidonakis, these proceedings.
- [30] S. Chekanov *et al.* [ZEUS Collaboration], arXiv:0806.0807, to be published in Phys. Rev. Lett. and U. Karshon, these proceedings.
- [31] M. Althoff *et al.* [TASSO Collaboration], Phys. Lett. B **121** (1983) 216; M. Acciarri *et al.* [L3 Collaboration], Phys. Lett. B **501** (2001) 173.
- [32] R. De Vita, these proceedings.
- [33] G.P. Gilfoyle, these proceedings.
- [34] A. Adare *et al.* [Phoenix Collaboration], Phys. Rev. C **78** (2008) 014901 [arXiv:0801.4545] and H. Caines, these proceedings.
- [35] S. Chekanov *et al.* [ZEUS Collaboration], JHEP **0806** (2008) 061 and T. Tymieniecka, these proceedings.
- [36] F.D. Aaron *et al.* [H1 Collaboration], Phys. Lett. B **654** (2007) 148 and D. Traynor, these proceedings.
- [37] A. Falkiewicz, these proceedings.
- [38] A. Białas and M. Jeżabek, Phys. Lett. B **590** (2004) 233.
- [39] T. Tymieniecka, these proceedings.
- [40] G. Gapienko, these proceedings.
- [41] S. Moch and A. Vogt, Phys. Lett. B **659** (2008) 290 [arXiv:0709.3899] and S. Moch, these proceedings.
- [42] S. Albino, B.A. Kniehl and G. Kramer, Nucl. Phys. B **803** (2008) 42 [arXiv:0803.2768] and B. Kniehl, these proceedings.
- [43] V.M. Abazov *et al.* [DZero Collaboration], arXiv:0804.1107 and M. Campanelli, these proceedings.
- [44] P. Aurenche, M. Fontannaz, J.P. Guillet, E. Pilon and M. Werlen, Phys. Rev. D **73** (2006) 094007 [hep-ph/0602133].
- [45] K. Nowak, these proceedings.
- [46] M. Fontannaz, J. P. Guillet and G. Heinrich, Eur. Phys. J. C **21** (2001) 303 [hep-ph/0105121]; M. Fontannaz and G. Heinrich, Eur. Phys. J. C **34** (2004) 191 [hep-ph/0312009].
- [47] A.V. Lipatov and N. P. Zotov, Phys. Rev. D **72** (2005) 054002 [hep-ph/0506044].
- [48] V.M. Abazov *et al.* [DZero Collaboration], arXiv:0802.2400 and M. Voutilainen, these proceedings.
- [49] P. Schieferdecker, these proceedings.
- [50] T. Namssoo, these proceedings.
- [51] E. Ron, these proceedings.
- [52] T. Theedt, these proceedings.
- [53] M. Gouzevitch, these proceedings.
- [54] Z. Nagy and Z. Trocsanyi, Phys. Rev. Lett. **87** (2001) 082001 [hep-ph/0104315].
- [55] A. Gehrman-De Ridder, T. Gehrman, E.W.N. Glover and G. Heinrich, JHEP **0712** (2007) 094 [arXiv:0711.4711].
- [56] A. Heister *et al.* [ALEPH Collaboration], Eur. Phys. J. C **35** (2004) 457.
- [57] G. Dissertori, A. Gehrman-De Ridder, T. Gehrman, E.W.N. Glover, G. Heinrich and H. Stenzel, JHEP **0802** (2008) 040 [arXiv:0712.0327] and H. Stenzel, these proceedings.
- [58] T. Gehrman, G. Luisoni and H. Stenzel, Phys. Lett. B **664** (2008) 265 [arXiv:0803.0695] and G. Luisoni, these proceedings.
- [59] T. Kluge, these proceedings.

- [60] G.P. Salam and G. Soyez, JHEP **0705** (2007) 086 [arXiv:0704.0292].
- [61] M. Cacciari and G.P. Salam, Phys. Lett. B **641** (2006) 57 [hep-ph/0512210].
- [62] J. Rojo, these proceedings [arXiv:0806.3958].
- [63] M. Cacciari, G.P. Salam and G. Soyez, JHEP **0804** (2008) 063 [arXiv:0802.1189] and G. Soyez, these proceedings.
- [64] M. Cacciari and G.P. Salam, Phys. Lett. B **659** (2008) 119 [arXiv:0707.1378];  
M. Cacciari, G.P. Salam and G. Soyez, JHEP **0804** (2008) 005 [arXiv:0802.1188] and M. Cacciari, these proceedings.